Molecular Biology of the Cell
Vol. 21, 1097–1110, March 15, 2010

Compartmentalized Cyclic Adenosine 3′,5′-Monophosphate at the Plasma Membrane Clusters PDE3A and Cystic Fibrosis Transmembrane Conductance Regulator into Microdomains

Himabindu Penmatsa,* Weiqiang Zhang,* Sunitha Yarlagadda,* Chunying Li,† Veronica G. Conoley,* Junming Yue,* Suleiman W. Bahouth,‡ Randal K. Buddington,§ Guangping Zhang,‖ Deborah J. Nelson,‖ Monal D. Sonecha,¶ Vincent Manganiello,# Jeffrey J. Wine,¶ and Anjaparavanda P. Naren*

*Department of Physiology, University of Tennessee Health Science Center, Memphis, TN 38163; †Department of Biochemistry and Molecular Biology, Wayne State University School of Medicine, Detroit, MI 48201; ‡Department of Pharmacology, University of Tennessee Health Science Center, Memphis, TN 38163; §Department of Health and Sports Sciences, University of Memphis, Memphis, TN 38152; ‖Department of Neurobiology, Pharmacology and Physiology, University of Chicago, Chicago, IL 60637; ¶Cystic Fibrosis Research Laboratory, Stanford University, Stanford, CA 94305; and #Division of Intramural Research, National Heart, Lung and Blood Institute, National Institutes of Health, Bethesda, MD 20892

Submitted August 4, 2009; Revised January 6, 2010; Accepted January 11, 2010
Monitoring Editor: Robert G. Parton

Formation of multiple-protein macromolecular complexes at specialized subcellular microdomains increases the specificity and efficiency of signaling in cells. In this study, we demonstrate that phosphodiesterase type 3A (PDE3A) physically and functionally interacts with cystic fibrosis transmembrane conductance regulator (CFTR) channel. PDE3A inhibition generates compartmentalized cyclic adenosine 3′,5′-monophosphate (cAMP), which further clusters PDE3A and CFTR into microdomains at the plasma membrane and potentiates CFTR channel function. Actin skeleton disruption reduces PDE3A–CFTR interaction and segregates PDE3A from its interacting partners, thus compromising the integrity of the CFTR-PDE3A–containing macromolecular complex. Consequently, compartmentalized cAMP signaling is lost. PDE3A inhibition no longer activates CFTR channel function in a compartmentalized manner. The physiological relevance of PDE3A–CFTR interaction was investigated using pig trachea submucosal gland secretion model. Our data show that PDE3A inhibition augments CFTR-dependent submucosal gland secretion and actin skeleton disruption decreases secretion.

INTRODUCTION

Cyclic adenosine 3′,5′-monophosphate (cAMP) and cyclic guanosine-3′,5′-monophosphate (cGMP) are important second messengers in the cells. Their levels have to be maintained precisely to regulate a variety of signaling cascades and cellular processes (e.g., metabolism, cell proliferation, and differentiation), secretion, vascular and airway smooth-muscle relaxation, and production of inflammatory mediators (Zaccolo, 2006; Thompson *et al.,* 2007). cAMP exerts its effects through activation of a limited number of effectors including cAMP-dependent protein kinase A (PKA), GTP-exchange protein EPACs (exchange proteins activated by cAMP) and via a cAMP-gated ion channel (Thompson *et al.,* 2007; Halpin, 2008). It is now appreciated that cAMP signaling in cells is compartmentalized, allowing control of signal transduction both spatially and temporally (Cooper, 2005; Conti and Beavo, 2007; Li *et al.,* 2007; Halpin, 2008). The concept of compartmentation of cAMP was formulated in the 1980s from the studies on cardiac myocytes (Buxton and Brunton, 1983). The idea was fully appreciated with the development of genetically encoded cAMP probes that directly visualize intracellular cAMP gradients (Zaccolo and Pozzan, 2002) and the discovery of A-kinase–anchoring proteins (AKAPs; Smith *et al.,* 2006). AKAPs have been shown to sequester PKA to distinct subcellular compartments and to position specific enzymes, e.g., cyclic nucleotide phosphodiesterases (PDEs), in close proximity to tightly regulate local cAMP levels (Baillie *et al.,* 2005). The role of PDEs in

This article was published online ahead of print in *MBC in Press* (http://www.molbiolcell.org/cgi/doi/10.1091/mbc.E09–08–0655) on January 20, 2010.

Address correspondence to: Anjaparavanda P. Naren (anaren@uthsc.edu).

Abbreviations used: AC, adenylyl cyclase; AKAPs, A kinase-anchoring proteins; AlphaScreen, amplified luminescent proximity homogeneous assay; BSA, bovine serum albumin; cAMP, cyclic adenosine 3′,5′-monophosphate; CF, cystic fibrosis; CFTR, cystic fibrosis transmembrane conductance regulator; COPD, chronic obstructive pulmonary disease; DSP, dithiobissuccinimidyl propionate; EPAC, exchange protein activated by cAMP; FRET, fluorescence resonance energy transfer; IBMX, isobutylmethylxanthine; $I_{sc,}$ short-circuit current; MSD, mean squared displacement; N-FRET, normalized FRET; N-FRETc, the normalized corrected FRET; PDE, phosphodiesterase; PDE3A, phosphodiesterase type 3A; PDE3B, phosphodiesterase type 3B; PDE4, phosphodiesterase type 4; PKA, protein kinase A; SPT, single-particle tracking.

compartmentalized cAMP signaling has been investigated for PDE4 isoforms, e.g., the PDE4D5 isoform has been shown to form macromolecular complexes with β_2-adrenergic receptor (β_2AR) and scaffolding protein, β-arrestins. On agonist stimulation, the translocation of PDE4/β-arrestin signaling complex to the plasma membrane results in the localized degradation of cAMP at its source of production (Perry *et al.*, 2002).

PDEs catalyze the hydrolysis of the 3′,5′-phosphodiester bond of cyclic nucleotides and thus play pivotal roles in regulating intracellular concentrations and downstream effects of secondary messengers (Beavo, 1995; Degerman *et al.*, 1997). PDEs have been reported to interact with regulatory proteins, scaffolding proteins, and other signaling molecules to form macromolecular complexes at specific cellular microdomains, which increases specificity and efficiency in cAMP signaling (Smith *et al.*, 2006; Conti and Beavo, 2007). Eleven families of mammalian PDEs (PDE1-11) have been reported. Most of the families have more than one member. Enzymes from the PDE4 family have attracted particular interest as they provide therapeutic targets for diseases such as asthma or chronic obstructive pulmonary disease (COPD). PDE4 isoforms such as PDE4D3 and PDE4D5 have been shown to be involve in compartmentalized cAMP signaling by forming complexes with PKA, AKAPs, and other signaling components (Perry *et al.*, 2002; Asirvatham *et al.*, 2004; Baillie *et al.*, 2005). The PDE3 family has two isoforms, PDE3A and PDE3B. PDE3s have distinctive characteristics that distinguish them from other PDEs, e.g., an insert of 44 amino acids in the catalytic domain and six hydrophobic putative transmembrane domains at the N terminus. The structural organization of PDE3A and PDE3B protein is identical. However, the two isoforms exhibit tissue-specific expression and distinct cellular distributions (Meacci *et al.*, 1992; Degerman *et al.*, 1997; Conti and Beavo, 2007). PDE3A is the major isoform expressed in the heart, lung, and platelets, where it regulates physiological processes such as contraction, relaxation, and platelet aggregation (Shakur *et al.*, 2001). PDE3B is highly expressed in hepatocytes, adipocytes, and beta cells and has been identified as a potential target for the treatment of obesity and diabetes (Thompson *et al.*, 2007). Specific PDE3 inhibitors, presumably by inhibiting PDE3A, have been reported to enhance myocardial contractility and induce vascular and airway smooth-muscle relaxation and have been used to treat heart failure and intermittent claudication (Liu *et al.*, 2001; Shin *et al.*, 2007; Halpin, 2008).

CFTR is a cAMP-regulated chloride channel localized primarily at the apical surfaces of epithelial cells lining airway, gut, and exocrine glands, where it is responsible for transepithelial salt and water transport (Riordan *et al.*, 1989; Anderson *et al.*, 1991; Bear *et al.*, 1992). CFTR function is also critical in maintaining fluid homeostasis, airway fluid clearance, and tracheal mucosal secretion in healthy and disease phenotypes (Wine and Joo, 2004; Riordan, 2008). A growing number of studies suggest that CFTR interacts directly or indirectly with other transporters, ion channels, scaffolding proteins, protein kinase, and cytoskeletal elements to form macromolecular complexes (Naren *et al.*, 2003; Yoo *et al.*, 2004; Li and Naren, 2005; Li *et al.*, 2005). Recently, we demonstrate the spatiotemporal coupling of a cAMP transporter, multidrug resistance protein 4 (MRP4), to CFTR Cl^- channel function in the gut epithelia and its importance in compartmentalized cAMP signaling (Li *et al.*, 2007).

CFTR is regulated by the activities of adenylyl cyclases (ACs) and PDEs via the activation of PKA. Inhibition of PDE4 and/or PDE3 has been demonstrated to activate CFTR Cl^- channel function (Kelley *et al.*, 1995, 1997; O'Grady *et al.*, 2002; Cobb *et al.*, 2003; Barnes *et al.*, 2005; Liu *et al.*, 2005; Lee *et al.*, 2007). However, most of this research was focused on functional association between PDEs and CFTR by using electrophysiological techniques. The results are still controversial regarding which isoform is the major regulator for CFTR channel function. Recently, Lee *et al.* (2007) demonstrated a physical association between PDE4D and CFTR and proposed a mechanism for PDE4D regulation of CFTR channel function. The physical interaction between other PDEs, especially PDE3 isoforms, and CFTR and the molecular mechanism through which these functional interactions occur remain unsolved.

Herein, we are the first to demonstrate that PDE3A physically and functionally interacts with the CFTR channel. Inhibition of PDE3A generates compartmentalized cAMP, which further clusters PDE3A and CFTR into microdomains at the plasma membrane and augments CFTR channel function including tracheal submucosal gland secretion. We also show that disruption of CFTR-PDE3A–containing macromolecular complexes abolishes compartmentalized cAMP signaling. Consequently, PDE3A inhibition no longer activates CFTR channel function in a compartmentalized manner.

MATERIALS AND METHODS

Reagents

Cilostazol and rolipram were purchased from Biomol (Plymouth Meeting, PA). Forskolin was obtained from Tocris (Ellisville, MO). Dithiobissuccinimidyl propionate (DSP) was obtained from Pierce (Rockford, IL). Adenosine, IBMX, cpt-cAMP, latrunculin B (Lat B), carbachol, and indomethacin were purchased from Sigma-Aldrich (St. Louis, MO).

Cell Culture and Transfections

HEK293 cells were cultured in DMEM-F12 media (Invitrogen, Carlsbad, CA) containing 10% serum and 1% penicillin/streptomycin and maintained in 5% CO_2 incubator at 37°C. Calu-3 cell line was purchased from ATCC (Manassas, VA) and cultured in MEM media (Invitrogen) containing 15% serum, 1% penicillin/streptomycin, 1 mM sodium pyruvate, and 1× nonessential amino acids. Lipofectamine 2000 (Invitrogen) was used to express plasmids containing CFTR or PDE3A in both HEK293 and Calu-3 cell lines according to manufacturer's instructions. Stable cell lines were generated by selection using 0.4 mg/ml G418 (geneticin).

Cloning

Full-length PDE3A was cloned into pcDNA3.1(−) containing yellow fluorescent protein (YFP) or cyan fluorescent protein (CFP), thereby generating pcDNA3.1(−)-CFP-PDE3A and pcDNA3.1(−)-YFP-PDE3A. Toward this, primers were designed with XhoI and Asp7181 sites at the 5′ and 3′ end of full-length PDE3A. A Flag or hemagglutinin (HA) tag was inserted in the putative first outer loop of full-length PDE3A between amino acids 104 and 105 using site-directed mutagenesis. Site-specific primers were designed with Flag or HA sequence in the middle of the primer and the double-stranded plasmid containing full-length PDE3A was mutated using PCR with QuikChange II site-directed mutagenesis kit (Stratagene, La Jolla, CA). Primer design and reaction conditions were according to the protocol recommended by the manufacturer. Human PDE3A constructs spanning the whole protein (1-255, 255-750, 751-1035, and 1035-1141 aa) were PCR-amplified. The PCR-cleaned DNA was further used for ligation-independent cloning (LIC) in pTriEx-4 and pET-41 vectors using Ek/LIC cloning kit from Novagen (EMD Chemicals, Gibbstown, NJ).

Submucosal Gland Secretion

Submucosal gland secretion was monitored as described by Wine's lab (Joo *et al.*, 2001). Freshly collected pig trachea was placed in cold Krebs-Ringer bicarbonate buffer (120 mM NaCl, 25 mM $NaHCO_3$, 3.3 mM KH_2PO_4, 0.8 mM K_2HPO_4, 1.2 mM $MgCl_2$, 1.2 mM $CaCl_2$, 10 mM D-glucose, and 1 μM indomethacin). The submucosal layer was carefully dissected from the cartilage, and a 1-cm piece was mounted in a chamber with the mucosal side up. The mucosal side was wiped and quickly air-dried with 95% O_2 and 5% CO_2 gas. A thin layer of water-saturated mineral oil was applied to the mucosal side. The tissue was constantly maintained at 37°C and gassed with 95% O_2 and 5% CO_2 after mounting. To establish a baseline, Krebs-Ringer bicarbonate buffer

was added to the serosal side. The PDE3 inhibitor cilostazol (100 μM), CFTRinh-172 (50 μM), Lat B (10 μM), or cilostazol (100 μM)/Lat B (10 μM) were added to the serosal side after monitoring basal secretion. Carbachol (10 μM) was added at the end of the experiment to check for the viability of submucosal glands. Images were collected at 1-min time intervals with a digital camera (Motic Images 2.0 ML software, Richmond, BC, Canada) attached to a stereoscopic microscope (National Optical, San Antonio, TX) and analyzed using ImageJ software (NIH; http://rsb.info.nih.gov/ij/). A 1 × 1-mm grid was placed on the tissue in the last image for area measurements. Volume was calculated from area using the formula $v = \Pi r^3$, and the secretion rate was calculated as slope of volume-versus-time plot by fitting at least four points using linear regression.

Immunohistochemistry and Immunofluorescence Microscopy

Pig trachea were paraffin-embedded and sectioned. The slides with sections were treated with protease to retrieve the antigen. The antigens sections were blocked with PBS (containing 4% bovine serum albumin [BSA] and 0.2% Triton X-100) inside a humidifying chamber for 2 h. The slides were treated with rabbit polyclonal α-PDE3A (Santa Cruz Biotechnology, Santa Cruz, CA) at 1:50 dilution overnight. Normal rabbit IgG was used for negative control. The slides were then treated for 1 h with secondary antibody α-rabbit AlexaFluor 488 (Invitrogen) at 1:500 dilution and 1:1000 dilution of propidium iodide. Images were taken on a Carl Zeiss confocal microscope (Thornwood, NY).

Calu-3 cells were grown on glass-bottom dishes and fixed with 3.7% paraformaldehyde. The fixed cells were blocked, treated with antibodies, and imaged as described above.

Short-circuit Current Measurements

Polarized lung serosal cells (Calu-3) monolayers were grown on Costar Transwell permeable supports (Cambridge, MA; filter area 0.33 cm^2) until they reached a resistance of ~1500 Ù and then mounted in an Ussing chamber. Short-circuit currents (I_{sc}) were measured as described previously (Li *et al.*, 2005). Epithelia were bathed in Ringer solution (in mM; Basolateral: 140 NaCl, 5 KCl, 0.36 K_2HPO_4, 0.44 KH_2PO_4, 1.3 $CaCl_2$, 0.5 $MgCl_2$, 4.2 $NaHCO_3$, 10 HEPES, 10 glucose, pH 7.2, $[Cl^-] = 149$), and low Cl^- Ringer solution (in mM; Apical: 133.3 Na-gluconate, 5 K-gluconate, 2.5 NaCl, 0.36 K_2HPO_4, 0.44 KH_2PO_4, 5.7 $CaCl_2$, 0.5 $MgCl_2$, 4.2 $NaHCO_3$, 10 HEPES, 10 mannitol, pH 7.2, $[Cl^-] = 14.8$) at 37°C, and gassed with 95% O_2 and 5% CO_2. The PDE3-specific inhibitor cilostazol (10–100 μM), the PDE4 inhibitor rolipram (2–10 μM), or a combination of both inhibitors was added to the apical and basolateral sides. Adenosine was added to the apical and basolateral sides. Forskolin (20 μM) was added to both sides for maximal response. CFTRinh-172 (20 μM) was added to the apical side. For I_{sc} measurements with actin cytoskeleton disruption of the cells, Lat B (1 μM) was added to both apical and basolateral sides after pretreating the cells with Lat B (1 μM) for 30 min.

Iodide Efflux Assay

Human embryonic kidney (HEK) 293 cells expressing wild-type CFTR were grown on 60-mm dishes. Forty-eight hours later, iodide efflux was monitored as previously described (Naren *et al.*, 2003). Briefly, cells were loaded for 60 min at room temperature with loading buffer (136 mM NaI, 137 mM NaCl, 4.5 mM KH_2PO_4, 1 mM $CaCl_2$, 1 mM $MgCl_2$, 10 mM glucose, 5 mM HEPES, pH 7.2). Extracellular NaI was washed away thoroughly (seven times) with efflux buffer (136 mM $NaNO_3$ replacing 136 mM NaI in the loading buffer), and cells were equilibrated for 1 min in a final 1-ml aliquot. The first four aliquots were used to establish a stable baseline in efflux buffer alone. Agonist (1 μM adenosine with or without 100 μM cilostazol) was added to the efflux buffer, and samples were collected every minute for 6 min in the continued presence of agonists (i.e., the efflux buffer used for subsequent replacements also contained agonists at the same concentration). The iodide concentration of each aliquot was determined using an iodide-sensitive electrode (Thermo Scientific, Waltham, MA) and converted to iodide content (nanomoles/minute). HEK293 parental cells in the presence of forskolin were used as a negative control.

Fluorescence Resonance Energy Transfer Microscopy and Data Analysis

For ratiometric fluorescence resonance energy transfer (FRET), Calu-3 cells or HEK293 cells expressing CFP-EPAC-YFP were grown on glass-bottom dishes (MatTek, Ashland, MA), washed twice with Hanks' balanced salt solution (HBSS), and mounted on an inverted Olympus microscope (IX51, U-Plan Fluorite 60× 1.25 NA oil-immersion objective, Melville, NY). Cells were maintained in HBSS in the dark at room temperature. After establishing the baseline, PDE inhibitors were added as indicated. Ratiometric FRET imaging was performed as described previously (Li *et al.*, 2007). Briefly, images were collected using cooled electron microscope (EM)-CCD camera (Hamamatsu, Bridgewater, NJ) controlled by Slidebook 4.2 software (Intelligent Imaging Innovations, Denver, CO). Light source used was 300-W xenon lamp with a neutral density filter. JP4 CFP/YFP filter set was used for image capture (Chroma, Brattleboro, VT), which includes a 430/25-nm excitation filter, a double dichroic beam splitter and two emission filters (470/30 nm for CFP and 535/30 nm for FRET emission) alternated by filter-change controller Lambda 10-3 (Sutter Instruments, Novato, CA). Time-lapse images were captured with 100–300-ms exposure time and 1-min time intervals. After background subtraction, multiple regions of interest (10–20) were selected (three to five cells) for data analysis using ratio module. The emission ratio (CFP/FRET) was obtained from CFP and FRET emission of background subtracted cells.

For direct sensitized emission FRET, HEK293 cells were transiently transfected with pcDNA3.1(−)-CFP-PDE3A, or pcDNA3.1(−)-YFP-CFTR or both using Lipofectamine 2000 (Invitrogen). Single transfected cells were used to acquire CFP- or YFP-only images for bleed-through calculations. Double-transfected cells were used for data collection using CFP/YFP filter sets. After acquiring images without PKA agonists as the 0 time point images, PKA-activating cocktail (in μM; forskolin 10, IBMX 100, cpt-cAMP 200) was added, and images were acquired at 2-, 4-, 6-, 8-, and 10-min intervals. FRET calculations were performed as described (Galperin and Sorkin, 2003). Corrected FRET (FRETc) was calculated on a pixel-by-pixel basis for the entire image by using the equation: FRETc = FRET − (0.5 × CFP) − (0.06 × YFP), where FRET, CFP, and YFP correspond to background-subtracted images of cells coexpressing CFP-PDE3A and YFP-CFTR acquired through the FRET, CFP, and YFP channels, respectively. The 0.5 and 0.06 are the fractions of bleed-through of CFP and YFP fluorescence through the FRET filter channel, respectively. FRETc was normalized with donor CFP intensity (FRETc/CFP) to give the normalized corrected FRET (N-FRETc). The intensity of FRETc images was presented in monochrome mode, stretched between the low and high renormalization values according to a temperature-based lookup table, with black indicating low values and white indicating high values. All calculations were performed using FRET module of the SlideBook 4.2 software (Intelligent Imaging).

Coimmunoprecipitation and Immunoblotting

For detection of PDE3A and PDE3B expression in Calu-3 cells using Western blotting, the cells were lysed in lysis buffer (1× PBS, containing 0.2% Triton X-100 and protease inhibitors 1 mM phenylmethylsulfonyl fluoride, 1 μg/ml pepstatin A, 1 μg/ml leupeptin, and 1 μg/ml aprotinin). The lysate was centrifuged at 16,000 × *g* for 10 min at 4°C, and the clear supernatant was mixed with 5× Laemmli sample buffer (containing 2.5% β-mercaptoethanol), denatured, subjected to SDS-PAGE on 4–15% gel (Bio-Rad, Hercules, CA), transferred to PVDF membrane, and immunoblotted for PDE3A using a α-PDE3A pAb (Santa Cruz) or for PDE3B using α-PDE3B pAb (Santa Cruz). Calu-3 cells overexpressing HA-PDE3A were lysed, and the clear supernatant was used to probe for HA-PDE3A using α-HA (Sigma) using the method described above. To knockdown PDE3A expression, we used PDE3A shRNA (Santa Cruz) in Calu-3 cells, lysed the cells and immunoblotted for PDE3A using a α-PDE3A pAb (Santa Cruz).

For detecting PDE3A localization in Calu-3 cells and HEK293 cells using Western blotting, the cells were washed with 1× PBS, harvested and pelleted at 600 × *g* for 5 min at 4°C. The pellet was resuspended in hypotonic lysis buffer (10 mM HEPES, 1 mM EDTA, protease inhibitor cocktail, pH 7.2) by incubation for 10 min. The suspension was homogenized at 4°C by 10 strokes in Dounce homogenizer, followed by 15 strokes in the presence of equal volume of sucrose buffer (500 mM sucrose, 1 mM EDTA, 10 mM HEPES, pH 7.2). The lysate was spun at 6000 × *g* for 20 min at 4°C to obtain postmitochondrial supernatant. Crude membrane was collected by centrifuging the supernatant at 100,000 × *g* for 45 min at 4°C. The pellet was resuspended in isotonic buffer (250 mM sucrose, 1 mM EDTA, 10 mM HEPES, pH 7.2) and immunoblotted for PDE3A using a PDE3A pAb (Santa Cruz) using the method described above.

For coimmunoprecipitation of CFTR and PDE3A, HEK293 cells transfected with Flag-CFTR and HA-PDE3A or only HA-PDE3A were lysed and centrifuged (16,000 × *g* for 10 min at 4°C) using the method described above. The clear supernatant was subjected to immunoprecipitation using α-Flag beads (Sigma). The immunoprecipitated beads were washed three times with lysis buffer, and the proteins were eluted from the beads using 5× Laemmli sample buffer (containing 2.5% β-mercaptoethanol). The eluates were immunoblotted for PDE3A using PDE3A mAb (Novus Biologicals, Littleton, CO). For immunoprecipitation of PDE3A and CFTR in Calu-3 cells, the cell lysate was immunoprecipited with α-PDE3A and blotted for CFTR. For immunoprecipitation of PDE3A and PDE4D in Calu-3 cells, the lysate was immunoprecipited with α-PDE4D pAb (Abcam, Cambridge, MA) and blotted for PDE3A. All these coimmunoprecipitation experiments were performed using the same protocol.

For detecting the minimum domain of PDE3A responsible for interacting with CFTR, we overexpressed HIS-S–tagged constructs of PDE3A spanning the whole protein and full-length Flag-CFTR in HEK293 cells. The total protein from the cell lysate was immunoprecipitated with α-Flag beads (Sigma) and probed with α-S-HRP (horse radish peroxidase; EMD Chemicals) using the method described above.

For immunoprecipitating cross-linked complex, cells expressing Flag-CFTR and HA-PDE3A or only Flag-CFTR were washed twice with 1× PBS (containing 0.1 mM calcium chloride and 1 mM magnesium chloride) and incu-

bated with or without Lat B (1 μM) for 30 min at 37°C. The cells were then treated with thiol-cleavable, amine-reactive, homobifunctional cross-linker DSP (1 mM) for 5 min. DSP was removed and RIPA buffer (140 mM NaCl, 1% Nonidet P40, 0.5% Na-deoxycholate, 0.1% Na-dodecyl sulfate, and 50 mM Tris-HCl, pH 8.0) containing protease inhibitor cocktail was added to quench the reaction and lyse the cells. The lysate was spun at 20,000 rpm for 10 min at 4°C. After taking 100 μl of total protein for input, the rest of the protein was immunoprecipitated using α-HA beads (Sigma) overnight. The beads were washed twice with RIPA buffer and the cross-linked complex was eluted with 100 mM glycine (pH 2.2) and quickly neutralized with 150 mM Tris (pH 8.8). For cleaving the disulphide bond of DSP and separating the proteins, 2.5% β-mercaptoethanol was added to the sample Laemmli buffer. The proteins were immunoblotted for CFTR using M3A7 CFTR mAb (Millipore, Billerica, MA).

For all the immunoblotting experiments, we loaded samples of equal amounts of total protein.

Surface-labeling Assay

Calu-3 cells expressing Flag- or HA-PDE3A were grown on 35-mm dishes, fixed with 3.7% formaldehyde for 10 min, blocked with 1% BSA for 30 min, and treated with α-Flag or α-HA HRP (0.2 μg/ml) for 90 min. The HRP substrate 1-step Ultra TMB (Pierce) was then added to the dishes for ~20 min, and the reaction was stopped by adding equal amount of 2 M H_2SO_4. The absorbance was read at 450 nm.

To detect the effects of PKA-phosphorylation on surface expression levels of PDE3A, Calu-3 cells expressing Flag-PDE3A were pretreated with forskolin (20 μM) for 10 min, fixed, surface-labeled, and then assayed as described above.

To detect the effects of Lat B on PDE3A surface expression levels, Calu-3 cells expressing HA-PDE3A were pretreated with Lat B (1 μM) for 30 min and then surface-labeled as described above.

Surface Biotinylation and Immunoblotting

HEK293 cells expressing HA-PDE3A were surface biotinylated with EZ-Link Sulfo-NHS-LC-Biotin (Pierce) for 1 h at 4°C, lysed, and immunoprecipitated using α-HA agarose beads (Sigma). The biotinylated purified HA-PDE3A was pulled down using streptavidin beads (Pierce) for 1 h at room temperature. The beads were spun down to collect unbound fraction, and the beads contained the bound fraction. The proteins were mixed with 5× Laemmli sample buffer (containing 2.5% β-mercaptoethanol), denatured, subjected to SDS-PAGE on 4–15% gel (Bio-Rad), transferred to PVDF membrane, and immunoblotted for PDE3A using PDE3A mAb (Novus Biologicals).

Single-Particle Tracking

Calu-3 cells stably expressing HA-PDE3A were grown on 35-mm glass-bottom dishes (MatTek). Cells were washed twice with PBS containing 6 mM glucose and 1 mM sodium pyruvate (PBS/Glu/NaPyr) and blocked with PBS/Glu/NaPyr containing 4% BSA for 10 min. Cells were then incubated with biotin α-HA antibody (1 μg/ml, Sigma) for 15 min, washed five times followed by a second incubation with streptavidin-conjugated Qdot-655 (0.1 nM, Invitrogen) for 2 min, washed extensively eight times, and immediately mounted on an Olympus inverted microscope (IX51). The images were captured with Hamamatsu EM-CCD camera at 1–3 frames per second for 1–3 min with 50-ms exposure time, 100× oil-immersion objective (NA 1.40), xenon (300-W lamp) light source, and SlideBook 4.2 software. Qdot 655-A BrightLine high brightness and contrast single band filter set (Semrock, Rochester, NY) was used for collecting data. Single-particle tracking (SPT) was done using the particle-tracking module of SlideBook 4.2 software, which generates trajectories and calculates the mean squared displacement (MSD). The diffusion coefficient (D) was calculated by linear squares fitting using points 1–5 on the MSD curve. Five to 10 cells were used for plotting histograms of the diffusion coefficient.

To monitor changes in lateral diffusion of PDE3A with cytoskeletal disruption, cells were pretreated with Lat B (1 μM, 30 min), and Lat B was also added to the buffer during the course of the experiment.

AlphaScreen Assay for PDE3A–CFTR Interaction

AlphaScreen FLAG (M2) detection kit (Perkin Elmer, Waltham, MA) was used to detect the interaction between purified full-length biotin-(HA)-PDE3A and Flag-wt-CFTR. In brief, starting from a 100 nM final concentration, biotin-(HA)-PDE3A was serially diluted (in 1/2 log dilution series) in assay buffer (1× PBS, 0.1% BSA, 0.05% Tween 20 [vol/vol], pH 7.2) containing Flag-wt-CFTR (100 nM final concentration). The resulting solutions were incubated at room temperature for 30 min. Each sample solution (15 μl) was transferred to a white opaque 384-well microplate (OptiPlate-384, Perkin Elmer) in triplicates and into which anti-FLAG (M2) acceptor beads (5 μl, 20 μg/ml final concentration) were added and incubated for 30 min at room temperature. Streptavidin donor beads (5 μl, 20 μg/ml final concentration) were then added and incubated for 2 h at room temperature. The plate was read on an EnVision 2103 Multilabel Reader (Perkin Elmer).

Cell-attached Single-Channel Recording

Single-channel recordings were obtained from Calu-3 cells as described previously (Li *et al.*, 2007). The pipette solution contained either forskolin or cilostazol (10–20 μM) to activate CFTR channels. Both bath and pipette solution contained (in mM) 140 *N*-methyl-D-glucamine, 140 HCl, 2 $CaCl_2$, 2 $MgCl_2$, and 10 HEPES, pH 7.4. Single-channel currents were recorded at a test potential of +80 mV (reference to the cell interior) delivered from the recording electrode, filtered at 100 Hz, and sampled at 2 kHz.

Statistical Analyses

Statistical analyses were done using Student's *t* test (two-tailed) or ANOVA (single-factor), and $p < 0.01$ or $p < 0.05$ was considered significant. All the results are represented as mean ± SEM, with n equaling the number of experiments.

RESULTS

PDE3A Inhibition Augments CFTR Function by Generation of Compartmentalized cAMP

Submucosal gland secretion plays important roles in maintaining airway and lung health. It is usually stimulated by agonists that elevate the cAMP or Ca^{2+} level and has been reported to be at least in part CFTR-dependent (Choi *et al.*, 2007; Ianowski *et al.*, 2008). To explore the physiological relevance of functional interaction between CFTR and PDE3A, we used the pig tracheal submucosal gland secretion model. Pig is considered a closer model to human cystic fibrosis (CF), and a CF pig model is available for studying CFTR function (Rogers *et al.*, 2008). After established basal secretion, a specific PDE3 inhibitor, cilostazol (100 μM), was added to the serosal side to inhibit PDE3A. Cilostazol has been approved for treatment of intermittent claudication since 1999 in the United States and for treatment of peripheral artery occlusive disease (PAOD) in Japan since 1988 (Thompson *et al.*, 2007). As shown in Figure 1A, upon PDE3A inhibition, we observed a threefold increase in mean mucosal secretion rate (from 0.5 nl/min per gland basal secretion rate to 1.5 nl/min per gland). This increased secretion was inhibited by treatment of the trachea with a specific CFTR channel inhibitor, CFTRinh-172 (50 μM), suggesting that the increased secretion is CFTR-dependent. Carbachol, an agonist that stimulate the glands secretion by elevating Ca^{2+} level, was added at the end of the experiments to check for the viability of submucosal glands (Figure 1A).

The expression and localization of PDE3A in pig trachea was studied by immunohistochemical analysis using a PDE3A-specific polyclonal antibody and α-rabbit AlexaFluor 488 as the secondary antibody. We also investigated the localization of PDE3A in Calu-3 cells, a widely used model for submucosal gland serous cells (Ianowski *et al.*, 2008). Nonimmune rabbit IgG was used as negative control in these studies. As can be seen in Figure 1B, PDE3A is primarily localized at the plasma membrane of epithelial cells of pig trachea and at the plasma membrane of Calu-3 cells. It is to be noted that CFTR is also expressed at the plasma membrane of Calu-3 cells (Naren *et al.*, 2003; Li *et al.*, 2004, 2005).

To investigate if the functional interaction of PDE3A and CFTR can be observed in live cells, we used two CFTR Cl^- channel function assays. The first one was to measure CFTR-dependent I_{sc} in polarized Calu-3 cells mounted in an Ussing chamber (Li *et al.*, 2007). Consistent with the observation of Drumm's group (Kelley *et al.*, 1995), PDE3A inhibition increased CFTR Cl^- channel function. In the presence of cilostazol (10–100 μM), we observed dose-dependent increase in CFTR-mediated currents that was inhibited by CFTRinh-172 (20 μM; Figure 2A, top left panel). Forskolin (20 μM), an adenylyl cyclase stimulator that elicits a global

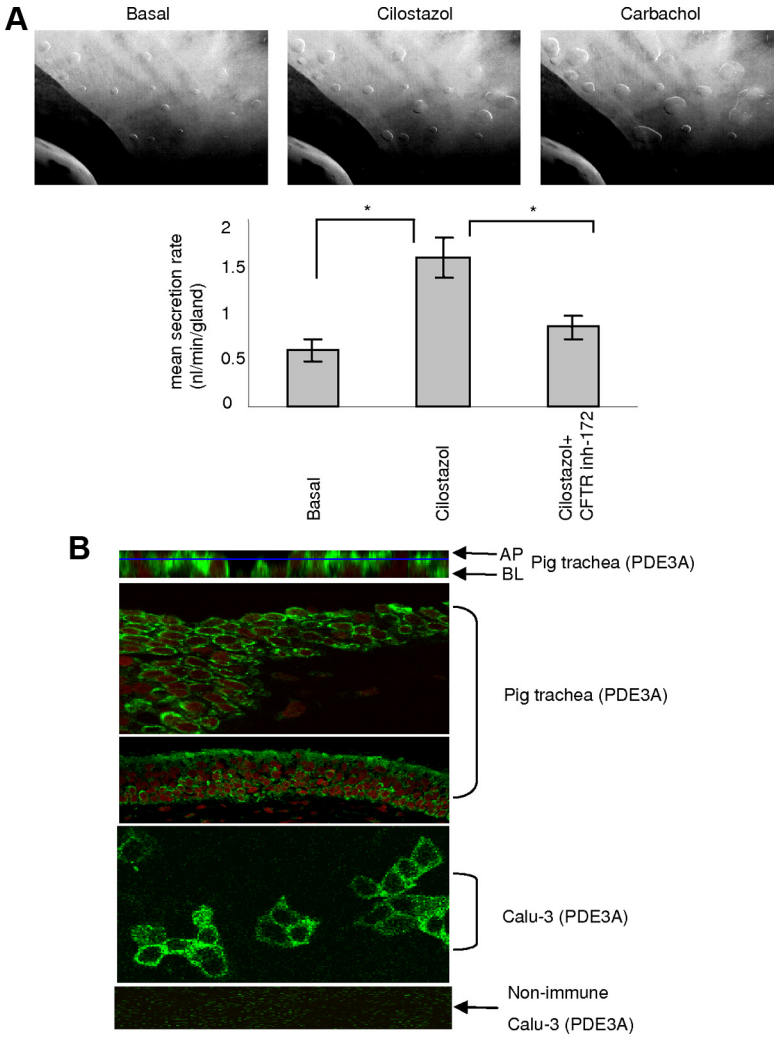

Figure 1. PDE3A inhibition augments CFTR function in pig trachea. (A) Representative images of submucosal gland secretion from pig trachea before (basal) and after addition of 100 μM cilostazol (time = 10 min) or 10 μM carbachol (time = 1 min). Bar graph is mean secretion rate ± SEM (n = 3 pigs, 12–35 glands, *p < 0.01) with cilostazol (100 μM) or with both cilostazol (100 μM) and CFTRinh-172 (50 μM). (B) Immunofluorescence micrographs for localization of PDE3A in Calu-3 cells and pig trachea. Apical (AP) and basolateral (BL) are x-z images and the rest are x-y images (green is PDE3A and red is nucleus).

increase of cAMP and maximally stimulates CFTR function (Li *et al.*, 2005. 2007) was used as positive control for the studies (Figure 2A, bottom left panel). It is to be noted that inhibition of PDE3A induced smaller magnitude of I_{sc} response compared with that stimulated by forskolin (20 μM). In the case of using cilostazol, the I_{sc} can be further increased to a maximal level by using forskolin (20 μM); possibly suggesting that inhibition of PDE3A generates localized cAMP rather than global cAMP. Because previous works demonstrated the regulatory role of PDE4 on CFTR channel function (Barnes *et al.*, 2005; Lee *et al.*, 2007), we also investigated the effect of rolipram (a PDE4-specific inhibitor) on CFTR-mediated short-circuit currents and observed a small increase in currents when compared with PDE3 inhibitor cilostazol (Figure 2A, top right and middle right panels; Supplemental Figure S6A). Interestingly, when both PDE3 and PDE4 inhibitors were used, we observed a synergistic increase in CFTR-mediated short circuit currents (Figure 2A, bottom right panel; Supplemental Figure S6A).

The second CFTR functional assay we used was to measure the iodide efflux from HEK293 cells overexpressing Flag-wt-CFTR. Adenosine was used to activate CFTR channel function in these studies, and HEK293 parental cells stimulated by forskolin were used as negative control. As can be seen in Figure 2B, inhibition of PDE3A increases CFTR-mediated iodide efflux. In the presence of cilostazol (100 μM), the iodide efflux increased >50% when a low dose of adenosine (1 μM) was used. Adenosine is a cAMP-elevating ligand that has been reported to stimulate CFTR channel function in a compartmentalized manner at the apical cell membranes when being used at low concentrations (<20 μM; Huang *et al.*, 2001; Li *et al.*, 2007).

The expression and localization of PDE3A in HEK293 cells and Calu-3 cells was studied by Western blotting. We used multiple antisera to show the expression of PDE3A in endogenous and overexpression conditions (Figure 2C, top left and top right panels).The immunoblot for crude membrane showed that PDE3A is expressed in the membrane of these cells (Figure 2C, bottom left panel). We also used PDE3A shRNA to knock down PDE3A expression and observed about a 50% knockdown in its expression (Figure 2C, top middle panel).We also investigated if PDE3B is expressed in Calu-3 cells endogenously, and we found very little expression at protein level (Figure 2C, bottom middle panel). 3T3-L1 cell lysate was used as positive control.

To characterize the localization of cAMP upon PDE3A inhibition and to investigate the possible mechanism through which CFTR functionally interacts with PDE3A, a FRET-based cAMP sensor, CFP-EPAC-YFP, was transfected into Calu-3 cells or HEK293 cells and then subjected to ratiometric FRET measurements. This highly sensitive, unimolecular fluorescent cAMP indicator allows to monitor cAMP dy-

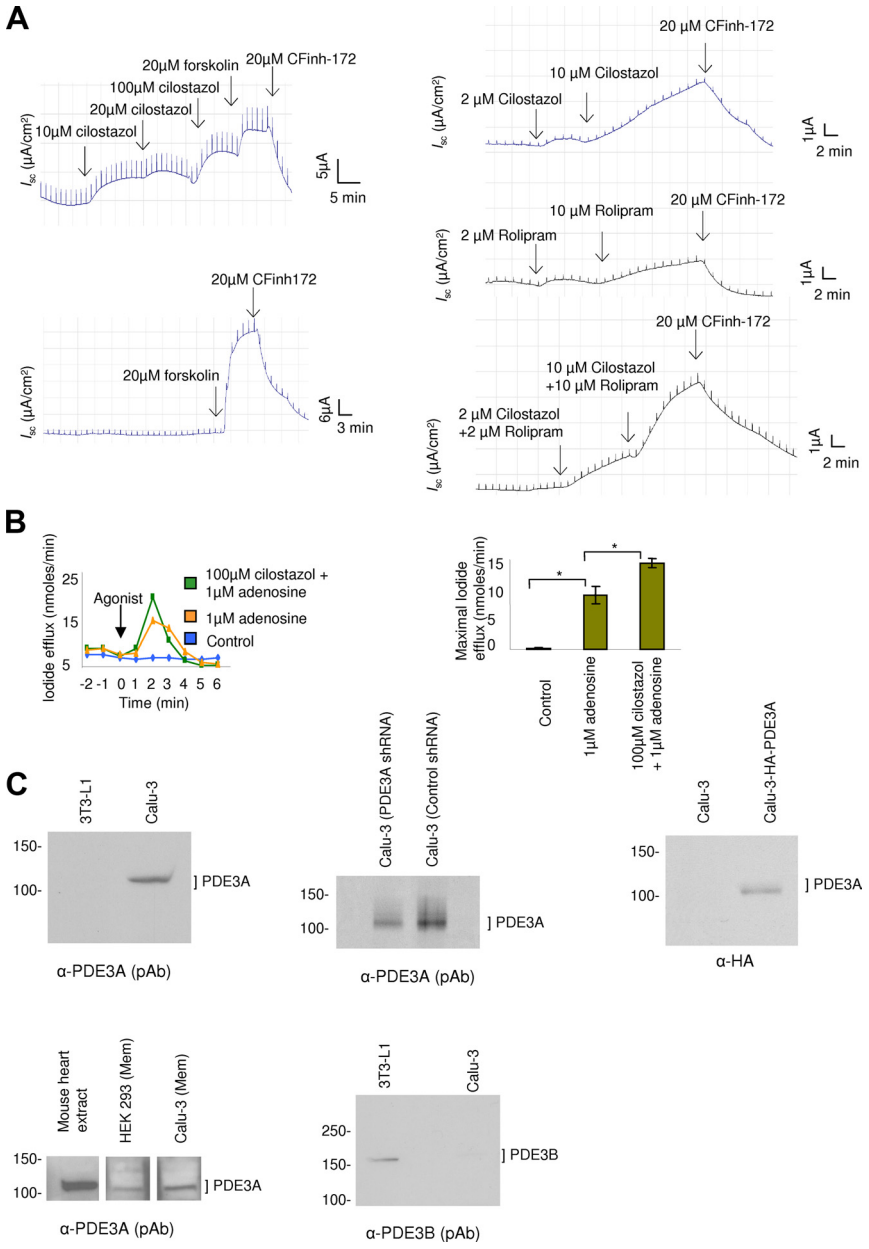

Figure 2. PDE3A inhibition augments CFTR function in Calu-3 and HEK293 cells. (A) Representative CFTR-dependent short-circuit currents (I_{sc}) with the addition of PDE3 inhibitor cilostazol (top left panel), or PDE4 inhibitor rolipram (middle right panel), or a combination of cilostazol and rolipram (bottom right panel). Forskolin or CFTRinh-172 was added at the end of the experiment. (B) Representative iodide efflux in HEK293 cells overexpressing CFTR in response to adenosine (±PDE3 inhibitor); bar graphs represent mean maximal iodide efflux at 2 min after adding agonist ± SEM (n = 3–5, *p < 0.01). (C) Immunoblots for PDE3A and PDE3B expression in Calu-3 cells using α-PDE3A pAb (top left panel) and α-PDE3B pAb (bottom right panel). Immunoblot for HA-PDE3A in Calu-3 cells expressing HA-PDE3A using α-HA antibody (top right panel). Immunoblot for PDE3A expression in crude membrane of Calu-3 cells and HEK293 cells using α-PDE3A pAb, mouse heart extract was used as control (bottom left panel). Immunoblot to show PDE3A expression knockdown with PDE3A shRNA in Calu-3 cells (top middle panel).

namics in intact cells, with very high temporal and spatial resolution (Ponsioen *et al.*, 2004; Li *et al.*, 2007). As can be seen from Figure 3 and Supplemental Figure S3, in Calu-3 cells, cAMP levels (represented by CFP/FRET emission ratio) increase upon PDE3A inhibition by using cilostazol. More importantly, the increase of cAMP levels occurs mainly at the edge area of the cells, suggesting a highly compartmentalized cAMP accumulation at the plasma membrane. Forskolin was used as a control that elicited a globe increase of cAMP (indicated by the uniform increase of the emission ratio in the entire cytoplasm). We also used this cAMP sensor in HEK293 cells to study if we can monitor a similar response upon PDE3A inhibition. As expected, we observed a dose-dependent increase in compartmentalized cAMP (Supplemental Figure S2). Interestingly, addition of rolipram (10 μM) induces a maximal increase in cAMP levels that is similar to the effect seen with forskolin stimulation (20 μM; Supplemental Figure S2). The data suggests that PDE3A is probably involved in compartmentalized cAMP signaling in these cells.

Taken together, our data show that PDE3A functionally interacts with CFTR channel. Inhibition of PDE3A augments CFTR function by generation of highly compartmentalized cAMP at the plasma membrane of airway epithelial cells.

PDE3A Interacts with CFTR in Live Cells in a PKA-dependent Manner

Given the functional interaction between PDE3A and CFTR channel, we continued to investigate whether or not a physical interaction exists, and therefore we cotransfected HEK293 cells with CFP-PDE3A and YFP-CFTR and measured the direct sensitized emission FRET in live cells. As shown in Figure 4, the two proteins interact at the plasma membrane as indicated by the FRET signals. More importantly, this interaction increased by almost 70% (normalized FRET) upon treatment with a PKA-activating cocktail (in

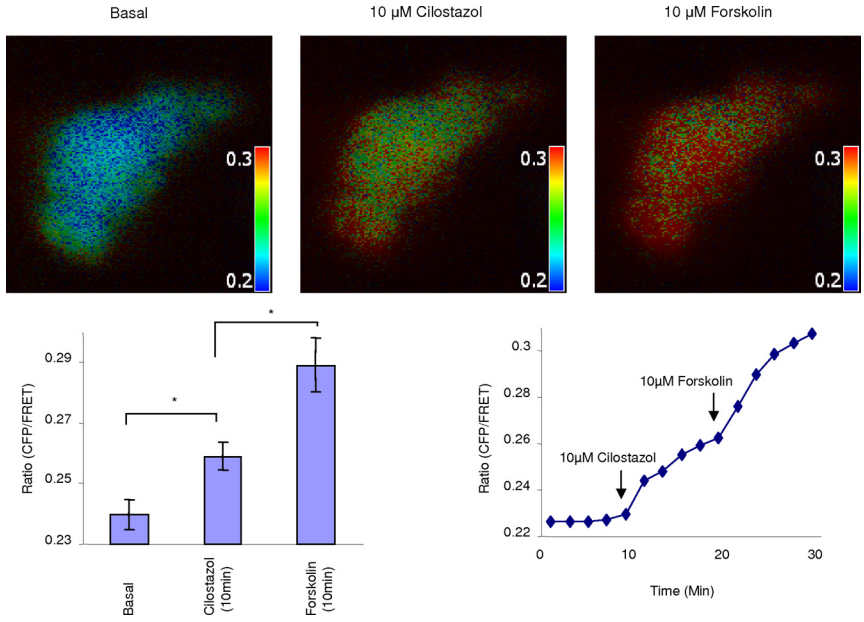

Figure 3. PDE3A inhibition generates compartmentalized cAMP at the plasma membrane of Calu-3 cells. Representative pseudocolor images of CFP/FRET emission ratio before (time = 0 min) and after adding 10 μM cilostazol or 10 μM forskolin (time = 10 min). Look up bar shows magnitude of emission ratio. Line graph is a representative graph for CFP/FRET emission ratio change with time upon adding agonist. Bar graph is mean ratio change ± SEM (n = 6 separate experiments, *$p < 0.05$).

μM; forskolin 10, IBMX 100, and cpt-cAMP 200), suggesting that the interaction between CFTR and PDE3A is PKA-dependent. Phosphorylation increases the binding between PDE3A and CFTR.

Coimmunoprecipitation and immunoblotting were also used to detect the interaction between PDE3A and CFTR under native and overexpression conditions. HEK293 cells were cotransfected with HA-PDE3A and Flag-CFTR, immunoprecipitated using α-Flag beads, and immunoblotted for PDE3A. Cells transfected with HA-PDE3A were used as negative control. For these protein interaction studies, we generated PDE3A constructs with either Flag or HA tag on the first outer loop at position 104 and CFTR with Flag tag at position 901 on the fourth outer loop (Figure 5A). As shown in Figure 5B (top left panel), HA-PDE3A can be coimmunoprecipited with Flag-CFTR, suggesting interaction exists between these two proteins, which corroborate the FRET data. We also tested the interaction under native conditions in Calu-3 cells and observed that CFTR coimmunoprecipitates with PDE3A (Figure 5B, top right panel). Given the fact that PDE3B is poorly expressed in Calu-3 cells, we overexpressed Flag-tagged PDE3B in HEK293 cells to study if it coimmu-

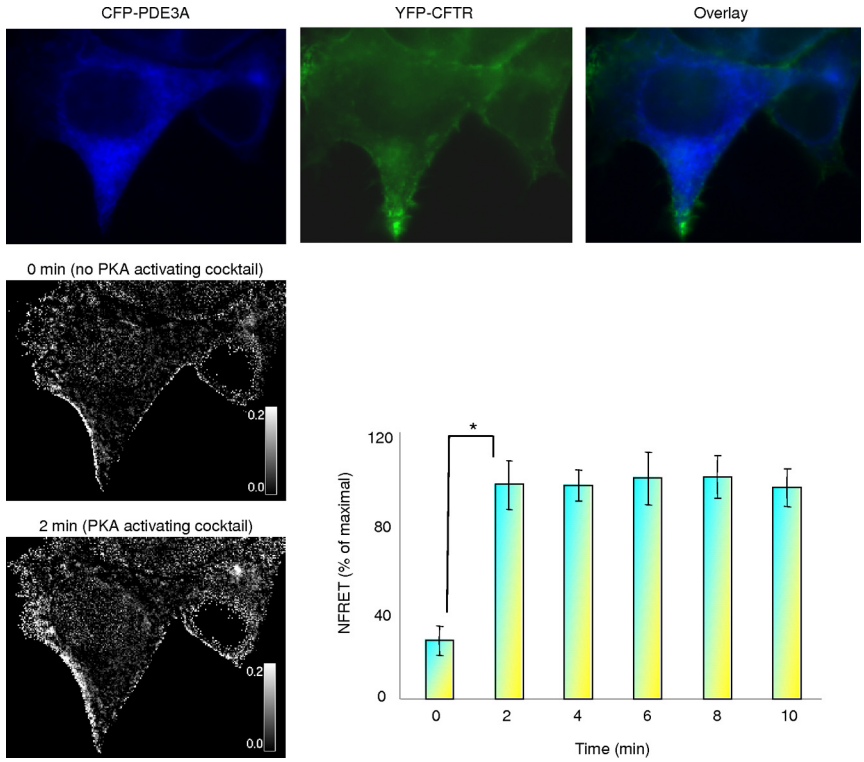

Figure 4. PDE3A interacts with CFTR in live cells in a PKA-dependent manner. Representative direct sensitized FRET between PDE3A and CFTR. HEK293 cells were cotransfected with CFP-PDE3A and YFP-CFTR, and the pseudocolor images show the expression. The intensity of N-FRETc (corrected and normalized) images was presented in monochrome mode, stretched between the low and high renormalization values, according to a temperature-based lookup table, with black indicating low values and white indicating high values. Bar graph is mean percentage of maximal increase in N-FRET ± SEM (n = 6 experiments, 12 regions of interest, and *$p < 0.01$).

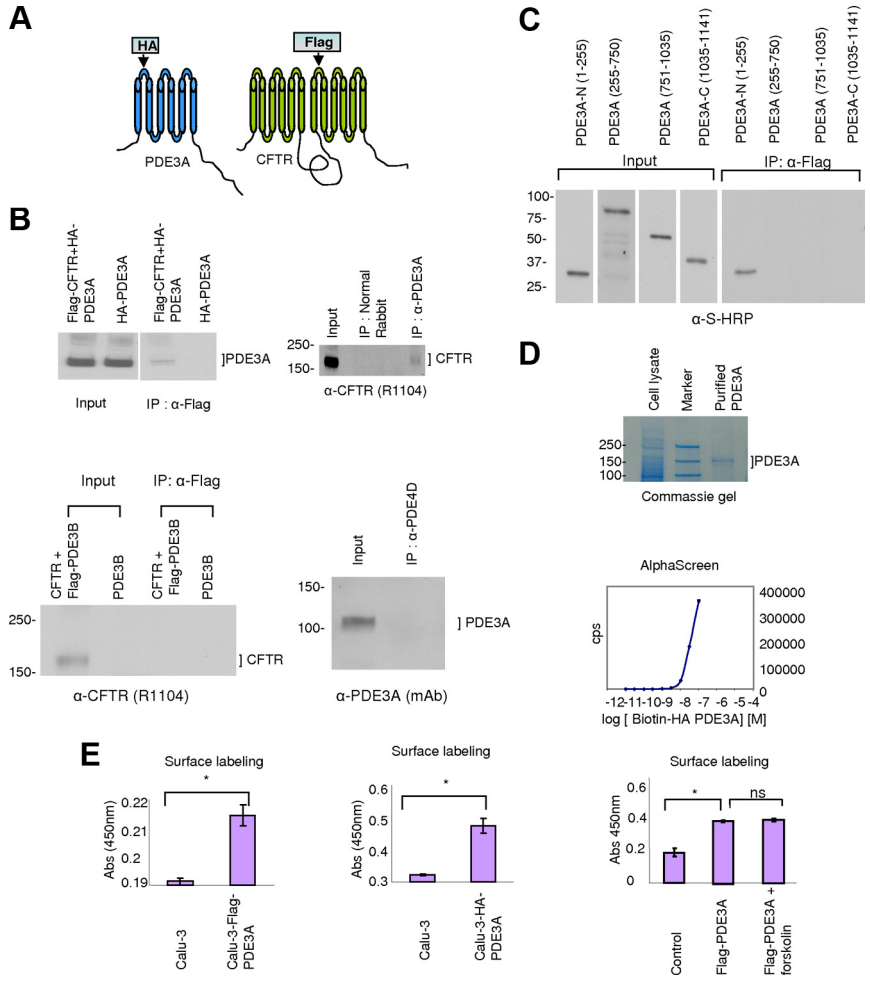

Figure 5. PDE3A interacts with CFTR. (A) Pictorial representation of tagged PDE3A and CFTR proteins that were generated with HA or Flag tag on the outer loop. (B) Coimmunoprecipitation of HA-PDE3A and Flag-CFTR in HEK 293 cells (top left panel). Immunoblot for CFTR and PDE3A interaction under native conditions in Calu-3 cells (top right panel). Normal rabbit antibody was used as negative control. Immunoblot for CFTR interaction with Flag-tagged PDE3B under overexpression conditions shows no interaction (bottom left panel). Immunoblot for PDE3A and PDE4D coimmunoprecipitation under native conditions shows no interaction (bottom right panel). (C) Binding assay to determine the minimum domain of PDE3A interacting with CFTR. Input shows different length constructs of PDE3A and coimmunoprecipitation blot shows N-terminal domain of PDE3A interacts with CFTR. (D) AlphaScreen assay to detect binding between full-length Flag-CFTR and full-length biotinylated HA-PDE3A. Graph shows AlphaScreen signal in counts per second (cps) with increasing concentrations of PDE3A (10 pM–100 nM); CFTR concentration was kept constant at 100 nM (n = 3). The Coomassie-stained gel (top panel) shows that full-length biotinylated HA-PDE3A was prepared with high purity. (E) Surface labeling assay to detect the expression of tagged PDE3A in Calu-3 cells. The results show that tagged PDE3A is expressed on the plasma membrane of cells. α-HA-HRP, 0.2 μg/ml, or α-Flag-HRP was used (n = 6, *$p < 0.01$). The surface expression of PDE3A in Calu-3 cells is unaltered by treatment with PKA-activating agonist forskolin as shown in surface labeling assay (right panel; n = 3, *$p < 0.01$); ns, not significant.

noprecipitates with CFTR. The result show that CFTR cannot be coimmunoprecipitated with PDE3B, suggesting there is no physical interaction between these two proteins (Figure 5B, bottom left panel). Because PDE4D has been shown to regulate CFTR channel function (Barnes *et al.*, 2005; Lee *et al.*, 2007) and because our results demonstrate a similar regulatory role for PDE3A, it is interesting to investigate if PDE4D coimmunoprecipitates with PDE3A under native conditions. Our results show that PDE3A and PDE4D do not coimmunoprecipitate in Calu-3 cells (Figure 5B, bottom right panel). However, the possibility of PDE3A and PDE4D being in close proximity cannot be completely ruled out given the synergistic effect observed for PDE3 inhibitor and PDE4 inhibitor on CFTR function (Figure 2A).

To identify minimum domain of PDE3A responsible for interacting with CFTR, we made four constructs of PDE3A spanning the whole protein (1-255, 255-750, 751-1035, and 1035-1141 aa) with histidine and S-protein tags in pTriEx and expressed these constructs with full-length Flag-CFTR in HEK293 cells. Coimmunoprecipitation data show that the N-terminal domain (1-255 aa) of PDE3A interacts with CFTR (Figure 5C).

To investigate if the interaction between PDE3A and CFTR is direct, we purified full-length Flag-CFTR and full-length biotinylated HA-PDE3A (Figure 5D). Amplified luminescent proximity homogeneous assay (AlphaScreen) FLAG (M2) detection kit was used to study the interaction between these two purified proteins. AlphaScreen assay is a highly sensitive method that can be used to detect direct interactions between interacting partners at femtomolar concentrations (Ullman *et al.*, 1996). For these studies, we kept the Flag-CFTR concentration constant (100 nM final concentration) and used increasing concentrations of biotinylated HA-PDE3A (10 pM to 100 nM). As can be seen from Figure 5D, HA-PDE3A interacts directly with Flag-CFTR at nanomolar concentrations and in a dose-dependent manner.

To test whether the increased interaction between PDE3A and CFTR by PKA phosphorylation is due to the altered surface expression levels of PDE3A, we used a surface-labeling assay to study the expression of Flag- or HA-PDE3A at the plasma membrane of Calu-3 cells. Calu-3 cells endogenously expressing PDE3A were used as control. The formaldehyde-fixed cells were labeled with α-Flag-HRP or α-HA-HRP and incubated with the HRP substrate, one-step Ultra TMB. The reaction was stopped by addition of 2 M H_2SO_4, and absorbance was read at 450 nm. As shown in Figure 5E (left and middle panels), Flag- or HA-PDE3A is expressed at the plasma membrane of Calu-3 cells, and the tags are indeed on the outer loop of the protein. To further verify the surface expression of PDE3A, we surface-labeled HEK293 cells expressing HA-PDE3A with a cell-impermeable biotinylating reagent Sulfo-NHS-LC-biotin at 4°C, lysed the cells, and immunoprecipitated using α-HA agarose beads. The purified biotinylated HA-PDE3A was pulled down using streptavidin beads, and the bound and unbound fractions were immunoblotted for PDE3A. HEK293

parental cells were used as a negative control. We found that more than 90% of PDE3A is present at the plasma membrane of transfected HEK293 cells (Supplemental Figure S5). Next, we investigated the effects of PKA-phosphorylation on the surface expression levels of Flag-PDE3A. Calu-3 cells transfected with Flag-PDE3A were pretreated with PKA-activating agonist (forskolin, 20 μM) and then were subjected to surface labeling as described above. The results showed that PKA phosphorylation does not increase PDE3A surface expression levels, as indicated by the unchanged absorbance between forskolin pretreated cells and untreated cells (Figure 5E, right panel).

These results show that PDE3A and CFTR physically interact with each other at the plasma membrane of epithelial cells (e.g., Calu-3 cells). Inhibition of PDE3A generates highly compartmentalized cAMP, which further clusters PDE3A and CFTR into microdomains and augments CFTR channel function in a compartmentalized manner.

Cytoskeleton Disruption Reduces the Physical and Functional Interaction between PDE3A and CFTR

All the data described above suggest that PDE3A and CFTR form macromolecular complexes at the plasma membrane, which ensures the compartmentalized cAMP signaling. The next questions we asked are 1) can we dissociate the CFTR-PDE3A–containing macromolecular complexes at the plasma membrane and 2) would this dissociation alter specifically PDE3A-dependent CFTR Cl^- channel function? Actin cytoskeleton has been shown to be important for maintaining CFTR in highly restricted domains at the plasma membrane (Jin *et al.*, 2007). Actin filament organization has also been shown to play functional role in the activation and regulation of CFTR Cl^- channel function (Cantiello, 1996; Chasan *et al.*, 2002; Ganeshan *et al.*, 2007). Therefore, we continued to investigate the effects of cytoskeleton disruption on the physical and functional interaction between PDE3A and CFTR and compartmentalized cAMP signaling. Lat B, a specific actin-disrupting reagent that causes actin filament depolymerization, was used for these purposes.

We first investigated the effects of actin cytoskeleton disruption on HA-PDE3A dynamics in live Calu-3 cells by using the SPT method. SPT is a powerful method to study the dynamics of individual proteins in the plasma membrane of live cells (Dahan *et al.*, 2003; Chen *et al.*, 2006). HA-PDE3A (HA tag on the first outer loop at position 104) was labeled with biotin α-HA antibody and then conjugated to streptavidin-conjugated Qdot-655 for monitoring its lateral mobility on the plasma membrane. The mean diffusion coefficient of PDE3A (0.0025 $\mu m^2/s$) that we observed in this study is similar to that reported for CFTR (Bates *et al.*, 2006; Jin *et al.*, 2007), indicating the confined diffusion of PDE3A. When the cells were treated with Lat B (1 μM), a significant increase in the MSD and diffusion coefficient of PDE3A was observed (Figure 6A, mean diffusion coefficient: 0.0117 $\mu m^2/s$; a 4.7-fold increase compared with the untreated cells), which suggests that actin cytoskeleton disruption uncouples PDE3A from the CFTR-containing complex, causes it to move freely (with higher diffusion coefficient), and compromises the integrity of multiprotein complex .

To further investigate if the physical interaction between PDE3A and CFTR is reduced with cytoskeleton disruption, we cotransfected HEK293 cells with Flag-CFTR and HA-PDE3A and cross-linked these two proteins in live cells using DSP (1 mM) with or without Lat B treatment. The cells were then lysed in RIPA buffer (containing 1 M urea) to disrupt all interactions except antigen–antibody interactions, and the proteins were coimmunoprecipitated using

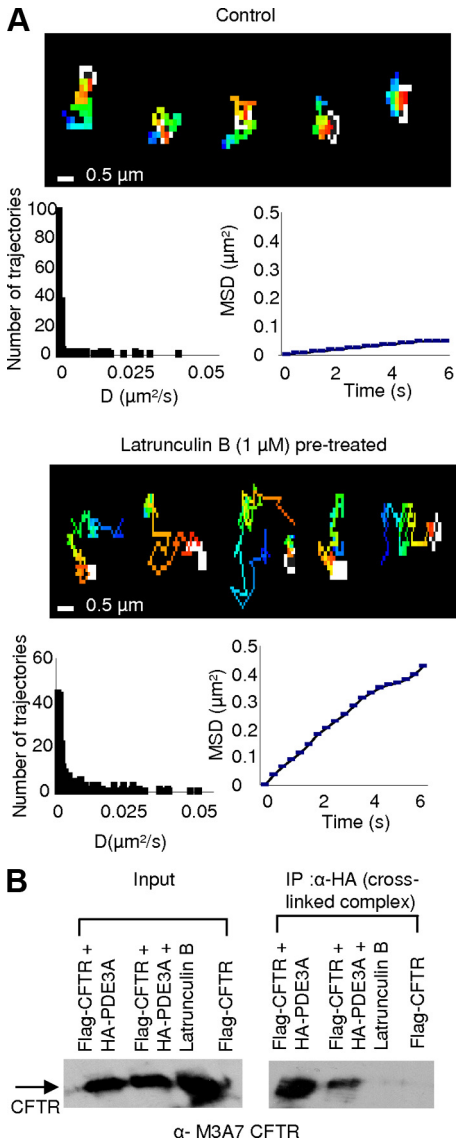

Figure 6. Actin depolymerization alters PDE3A dynamics and its physical coupling with CFTR. (A) SPT of HA-PDE3A in Calu-3 cells. Pseudocolor images show representative trajectories without or with Lat B (1 μM, 10 min) pretreatment. Histograms represent the diffusion coefficients, and MSD plots show representative mean squared displacement kinetics of HA-PDE3A in untreated and Lat B–pretreated cells (n = 6–9 cells, 150–230 trajectories). (B) Coimmunoprecipitation of HA-PDE3A and Flag-CFTR with or without Lat B pretreatment in HEK293 cells. The total protein from cells cotransfected with HA-PDE3A and Flag-CFTR was immunoprecipitated with α-HA beads and immunoblotted for CFTR. The experiment was repeated for three times.

α-HA beads and immunoblotted for CFTR. HEK 293 cells expressing only Flag-CFTR were used as negative control. DSP is a thiol-cleavable, amine-reactive homobifunctional cross-linker that has been used to cross-link proteins of interest in live cells (Li *et al.*, 2004). The result shows that Lat B treatment leads to a significant decrease in PDE3A–CFTR interaction (Figure 6B).

The data so far suggest that Lat B treatment does disrupt the PDE3A-CFTR–containing macromolecular complexes at the plasma membrane. We continued to test if the dissociation alters specifically PDE3A-dependent CFTR channel

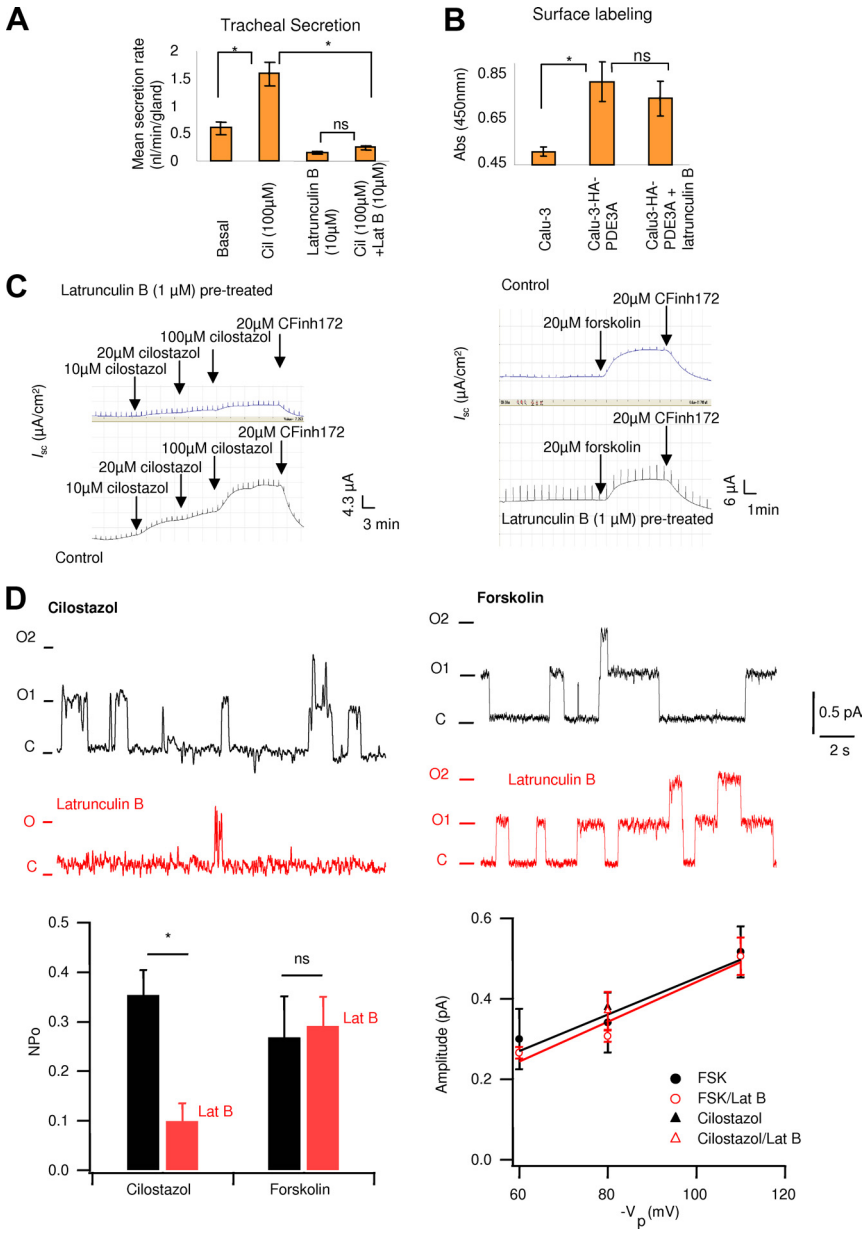

Figure 7. Actin depolymerization alters PDE3A dynamics and its functional interaction with CFTR. (A) Submucosal gland secretion from pig trachea before (basal) and after adding cilostazol (100 μM) with or without Lat B (10 μM). Bar graph is mean secretion rate ± SEM (n = 3 pigs, 30–35 glands, *p < 0.01). Student's *t* test was used within groups, and ANOVA was used between groups. cil, cilostazol; Lat B, Lat B; ns, not significant. (B) Surface expression of PDE3A is unaltered by Lat B pretreatment shown by surface labeling assay (n = 3, *p < 0.05); ns, not significant). (C) Representative CFTR-dependent I_{sc} traces for control and Lat B–pretreated cells showing response to cilostazol (left panel) and forskolin (right panel). (D) Representative single-channel CFTR currents recorded from cell-attached patches in cultured Calu-3 cells at a test potential of +80 mV. The top left current traces are representatives recorded in the presence of 10 μM cilostazol in the pipette solution. Current trace in red was recorded after incubation of the cells.

function. To test our hypothesis in a physiologically relevant system, we used Lat B in pig trachea submucosal gland secretion studies. As can be seen in Figure 7A, when treated with Lat B, a significant decrease (>90%) in cilostazol-activated and CFTR-dependent mean mucosal secretion was observed. We also observed that Lat B itself can cause a small decrease in the mean mucosal secretion rate. We ruled out the possibility of altered surface expression of PDE3A on Lat B treatment by using a surface-labeling assay that shows that the surface expression level of PDE3A is not significantly changed (Figure 7B).

CFTR-dependent I_{sc}s were measured in polarized Calu-3 cells mounted in an Ussing chamber. As shown in Figure 7C (left panel) and Supplemental Figure S6B, I_{sc} measurements in cells treated with Lat B show that the potentiating effects of PDE3A inhibition (cilostazol: 10–100 μM) on CFTR-dependent currents decreased by almost 65–80% compared with the cells without Lat B treatment. The data are consistent with the findings from pig tracheal submucosal gland secretion studies. It is to be noted that the maximally stimulated I_{sc} by forskolin (increases global cAMP) remains unaffected by Lat B treatment (Figure 7C, right panel). We also tested the effects of Lat B treatment on adenosine mediated CFTR-dependent I_{sc}. We found that in the presence of PDE3 inhibitor cilostazol adenosine-mediated CFTR-dependent I_{sc} are significantly inhibited by Lat B treatment, whereas the forskolin activated I_{sc} are not altered significantly (Supplemental Figure S4, A and B). These data further support our hypothesis that PDE3A is functionally and physically interacts with CFTR via compartmentalized cAMP. On actin cytoskeleton disruption by treatment of cells with Lat B, the CFTR–PDE3A interaction was decreased, and the coupling between PDE3A and CFTR is disrupted. As a result, the integrity of the CFTR-PDE3A–containing macromolecular complex is compromised and the compartmentalized cAMP signaling is abolished. Inhibition of PDE3A thus no longer potentiates CFTR Cl^- channel function in compartmentalized manner.

Results from cell-attached single-channel recording in Calu-3 cells strongly support our hypothesis and shed more mechanistic insights into the physical and functional interaction between PDE3A and CFTR and its actin cytoskeleton dependence. Cilostazol or forskolin was applied in the pipette to active CFTR channel function. As shown in Figure 7D (bottom right panel), there is no significant change in single-channel conductance for cells activated by either cilostazol or forskolin with or without Lat B treatment. CFTR channel open probability is significantly decreased in cilostazol-activated currents when treated with Lat B (Figure 7, top left panel). However, forskolin-activated currents were not altered with Lat B treatment (Figure 7, top right panel). These data clearly indicate that PDE3A inhibition activates CFTR channel function in a compartmentalized manner, and the interaction between these two proteins is actin cytoskeleton dependent.

Cumulatively, our findings provide clear evidence that, 1) PDE3A interacts physically and functionally with CFTR at the plasma membrane of airway epithelial cells (Calu-3); 2) inhibition of PDE3A generates high levels of compartmentalized cAMP that further clusters the two proteins into microdomain at the plasma membrane and potentiates CFTR Cl^- channel function; and 3) cytoskeleton disruption decreases CFTR–PDE3A interaction, scatters CFTR and PDE3A away from each other, and compromises the integrity of the macromolecular signaling complexes, leading to the loss of compartmentalized cAMP signaling. Consequently, inhibition of PDE3A no longer potentiates CFTR Cl^- channel function in a compartmentalized manner.

DISCUSSION

It is now well appreciated that the formation of multiple-protein macromolecular complexes at specialized subcellular microdomains increases the specificity and efficiency of signaling in cells (Baillie *et al.*, 2005; Li and Naren, 2005; Li *et al.*, 2007). The goals of this study are to investigate the physical and functional interaction between CFTR Cl^- channel and PDE3A, to uncover the molecular mechanism behind the interaction and to explore its physiological relevance in airway gland mucus secretion.

Physical and Functional Interaction between CFTR and PDE3A

In this study, we found that PDE3A is expressed at the plasma membrane of epithelial cells of pig trachea, Calu-3 cells, and HEK293 cells as supported by results from immunohistochemical analysis, Western blotting and cell surface labeling studies. We demonstrate that PDE3A directly interacts with CFTR in a PKA-dependent manner by using FRET, cross-linking, coimmunoprecipitation, and AlphaScreen assay. We identified that the N-terminal domain of PDE3A (1-255 aa) is responsible for interacting with CFTR. PDE3B, however, was found expresses poorly in Calu-3 cells and cannot be coimmunoprecipitated with CFTR in overexpression system. We also observed the functional interaction between PDE3A and CFTR Cl^- channel. Inhibition of PDE3A augments CFTR Cl^- channel function as seen in I_{sc} and iodide efflux measurements. Studies on cAMP localization and dynamics by using a FRET-based cAMP sensor, CFP-EPAC-YFP, show that, upon PDE3A inhibition, cAMP is generated in highly compartmentalized manner at the plasma membrane. All these data suggest that CFTR and PDE3A form macromolecular complexes at the plasma membrane, which establish the molecular basis for observed compartmentalized cAMP signaling. This hypothesis is further supported by the facts that actin cytoskeleton disruption decreases CFTR–PDE3A interaction, scatters CFTR and PDE3A away from each other and compromises the integrity of the macromolecular complexes. Consequently, inhibition of PDE3A no longer activates CFTR Cl^- channel function in compartmentalized manner, as evidenced by cell-attached single-channel recording studies, I_{sc} measurements, and pig tracheal submucosal gland secretion studies in the presence of Lat B, an actin skeleton-disrupting reagent. On the basis of these results, we propose a model to depict the mechanism through which the physical and functional interaction between PDE3A and CFTR Cl^- channel occurs (Supplemental Figure S1).

Association of PDEs with CFTR and Compartmentalized cAMP Signaling

PDEs have been shown to play vital roles in compartmentalized cAMP/PKA signaling processes. The emerging idea is that it is the compartmentalization of individual PDEs, rather than its total expression level, that is important in modulating localized intracellular cAMP levels (Zaccolo, 2006). AKAPs have been reported to play key roles in the assembly and organization of such compartmentalized cAMP/PKA signaling (Langeberg and Scott, 2005; McConnachie *et al.*, 2006). Taskén *et al.* (2001) reported that PDE4D3 and PKA form signaling complexes in the centrosomal area that are coordinated by centrosomal AKAP450 and regulate accurate spatiotemporal cAMP signals. Pozuelo Rubio *et al.* (2005) reported that PDE3A binds directly to 14-3-3 proteins in a phosphorylation-dependent manner and PDE3A also bind to plectin, a cytoskeletal linker protein. Recently, Puxeddu *et al.* (2009) demonstrated that PDE3A interacts with brefeldin A–inhibited guanine nucleotide-exchange proteins (BIG1 and BIG2) in HeLa cell cytosol and form BIG1- and BIG2-AKAP complexes that regulate ADP-ribosylation factors (ARFs) function via compartmentalized cAMP signaling.

PDE3 and PDE4 have been reported to be the major PDEs present in airway epithelial cells (Torphy, 1998; Wright *et al.*, 1998). Kelley *et al.* (1995) reported that CFTR-mediated Cl^- permeability is regulated by PDE3 in Calu-3 and 16HBE cells. They showed that inhibition of PDE3 in Calu-3 cells increases Cl^- efflux up to 13.7-fold, whereas rolipram (a specific PDE4 inhibitor) does not induce a significant increase. In another report, Kelly *et al.* (1997) showed that among several PDE inhibitors, the PDE3 inhibitor milrinone has the greatest effect on hyperpolarizing mouse nasal epithelium (an indicator of increased Cl^- secretion mediated by CFTR; ~7 mV). Rolipram was found to have a small but significant effect (~3 mV). The authors further demonstrated that ΔF508 CFTR can be in vivo activated in murine nasal epithelium by using a combination of forskolin and milrinone (Kelley *et al.*, 1997). O'Grady *et al.* (2002) reported that cAMP-dependent Cl^- secretion is regulated by multiple PDEs in human colonic epithelial cells (T84 cells). By measuring the I_{sc} of T84 monolayers grown on filter, the authors demonstrated that PDE3 and PDE1 are involved in regulating the rate of transepithelial Cl^- secretion. The effect of PDE4 inhibitor (RP-73401) on I_{sc} is significantly less potent than PDE3 inhibitors (milrinone, cilostamide, and trequinsin; O'Grady *et al.*, 2002). By measuring CFTR-dependent transepithelial I_{sc} in Calu-3 monolayer, Cobb *et al.* (2003) reported that PDE3 inhibitors (milrinone and cilostazol) and PDE4 inhibitor (rolipram) can elicit I_{sc}. They demonstrated that cilostazol and rolipram augment both the magnitude and the duration of I_{sc} after low-dose stimulation of adenosine receptor with adenosine. Their results suggest that in

addition to PDE3, other PDEs including PDE4 may play roles in regulating CFTR in Calu-3 cells (Cobb *et al.*, 2003). Recently, several reports suggest that PDE4 isoforms regulate CFTR channel function. Barnes *et al.* (2005) showed that PDE4D is localized in close proximity to CFTR at the apical membrane of airway epithelium. The authors demonstrated that PDE4 inhibitors (rolipram) stimulate CFTR channel function in excised apical patches of Calu-3 cells, whereas PDE3 inhibitor milrinone shows no significant effect. Their results suggest that PDE4 isozymes are critically involved in modulating the spread of cAMP signaling at the apical surface in Calu-3 cells and are the major regulators on CFTR channel function (Barnes *et al.*, 2005). Lee *et al.* (2007) demonstrated that a PDZ-containing protein, Shank2, negatively regulates CFTR channel function. The mechanism was suggested to be a competition between Shank2 and NHERF1 for binding to CFTR. Binding between Shank2 and CFTR breaches the CFTR–NHERF1 association and also brings PDE4D in the vicinity of CFTR, thus attenuating localized cAMP/PKA signals. PDE3 was shown not functionally associated with Shank2. This report may provide insights into the molecular mechanism for PDE4D accumulation in apical membrane. Liu *et al.* (2005) demonstrated the dynamic activation of CFTR by PDE3 and PDE4 inhibition in T84 cell monolayer by monitoring the Cl^- secretion using ^{125}I as tracer. Their data suggest that PDE3 and PDE4 (mainly PDE4D) form the major cAMP diffusion barrier in these cells.

Most of the previous works were focused on functional association between PDEs and CFTR. The results are controversial regarding which PDE isoform is the major regulator for CFTR channel. Moreover, the molecular basis and thus the mechanism behind the functional associations remain unsolved (except for the work from Lee *et al.*, 2007, who demonstrate a mechanism for PDE4D–CFTR association). Herein, we are the first to provide evidence that PDE3A directly interacts with CFTR. Our data suggest that PDE3A and CFTR form signaling macromolecular complexes at the plasma membrane of airway epithelial cells (Calu-3 cells). Other signaling components such as PKA, specific G protein–coupled receptors, G proteins, ACs, and AKAPs may also be present in the macromolecular complexes, which synergistically regulate compartmentalized cAMP signaling and specificity of CFTR activation. Interestingly, we also observed a synergistic effect of PDE3/PDE4 inhibition on CFTR channel activation. In considering of previous reports that show the regulatory roles for PDE4 and PDE3 on CFTR channel function, it is reasonable to suggest at this stage that both PDE3A and PDE4 are important regulators for CFTR function in airway epithelium. Also, it seems that they act through different mechanisms.

Physiological Relevance of CFTR–PDE3A Interaction in Airway Gland Mucus Secretion

Regulation of CFTR channel function via its interaction with PDEs is of physiological and pathophysiological importance owing to that 1) CFTR is the primary cAMP-activated Cl^- channel on the apical membrane of airway epithelia, thus playing critical roles in controlling the electrolyte/fluid balance and mucociliary clearance process (Pilewski and Frizzell, 1999); 2) phosphodiesterase inhibition remains a viable area of therapy for the treatment of airway diseases such as asthma and COPD (Chung, 2006). Submucosal glands secretion has been reported to play important roles in maintaining airway and lung health, and CFTR has been shown to play important roles in such processes. This idea is supported by the observations that CF glands have altered responses to secretagogues compared with normal glands (Ianowski *et al.*, 2008) and by the fact that in CF patients the airway host defense system is compromised, leading to chronic secondary bacterial infections and inflammation in the lung and respiratory failure (Pilewski and Frizzell, 1999; Sheppard and Welsh, 1999).

Drugs targeting PDEs are being considered for their cardiotonic, pulmonary vasodilator, smooth-muscle relaxant, antithrombotic, anti-inflammatory, and antiasthmatic properties (Conti and Beavo, 2007). Targeted inhibition of PDE4 has been pursued as a way of reducing inflammation in patients with asthma or COPD, diseases characterized by mucus-congested and inflamed airways (Barnette, 1999; Compton *et al.*, 2001). Cilomilast and roflumilast, two second generation PDE4 inhibitors, have shown potential benefits for treatment of asthma and COPD. However, clinical utility of PDE4 inhibitors has been limited by adverse effects including nausea, diarrhea, and vomiting (Chung, 2006; Halpin, 2008).

Although PDE3 inhibitors do not appear to have direct anti-inflammatory actions, they have been shown to augment the anti-inflammatory actions of PDE4 inhibitors (Schudt *et al.*, 1995; Giembycz *et al.*, 1996). Also, PDE3 inhibitors could act as bronchodilators and may have synergistic effects with PDE4 inhibitors (Halpin, 2008). Development of dual specificity inhibitors (such as dual PDE3-PDE4 inhibitors) may provide more bronchodilator and bronchoprotective effect in addition to the beneficial PDE4 effects (Giembycz, 2005). In this study, we show that PDE3A–CFTR interaction is physiologically relevant in pig tracheal submucosal gland secretion. We demonstrate that inhibition of PDE3A does increase the mean mucosal secretion rate in pig tracheal, which would be potentially beneficial in maintaining/restoring airway lung health.

In summary, our results clearly show that PDE3A functionally and physically interacts with CFTR. Inhibition of PDE3A generates compartmentalized cAMP, which further clusters PDE3A and CFTR into microdomains at the plasma membrane of epithelial cells and potentiates CFTR channel function. Our data suggest that PDE3A and CFTR form signaling macromolecular complexes at the plasma membrane of airway epithelial cells (Calu-3 cells), which establish the molecular basis for observed compartmentalized cAMP signaling. Our findings not only provide insights into the important roles of PDE3A in compartmentalized cAMP signaling and the molecular mechanism behind PDE3A–CFTR interaction, but may lay molecular basis for the development of dual specificity PDE3-PDE4 inhibitors for treatment of airway diseases such as asthma and COPD.

ACKNOWLEDGMENTS

We thank Dr. David Armbruster for critically editing the manuscript; Dr. Richard A. Heil-Chapdelaine for technical support with imaging; Dr. Bakhram K. Berdiev (Department of Cell Biology, University of Alabama at Birmingham, Birmingham, AL) for providing pcDNA3.1(−)-CFP and YFP-CFTR constructs; and Dr. Juan P. Ianowski for help with data analysis. This work was supported by grants from National Institutes of Health Grant DK074996 and DK080834 to A.P.N. and American Heart Association predoctoral fellowship R079008141 to H.P.

REFERENCES

Anderson, M. P., Gregory, R. J., Thompson, S., Souza, D. W., Paul, S., Mulligan, R. C., Smith, A. E., and Welsh, M. J. (1991). Demonstration that CFTR is a chloride channel by alteration of its anion selectivity. Science *253*, 202–205.

Asirvatham, A. L., Galligan, S. G., Schillace, R. V., Davey, M. P., Vasta, V., Beavo, J. A., and Carr, D. W. (2004). A-kinase anchoring proteins interact with phosphodiesterases in T lymphocyte cell lines. J. Immunol. *173*, 4806–4814.

Baillie, G. S., Scott, J. D., and Houslay, M. D. (2005). Compartmentalisation of phosphodiesterases and protein kinase A: opposites attract. FEBS Lett. *579*, 3264–3270.

Barnes, A. P., Livera, G., Huang, P., Sun, C., Oneal, W. K., Conti, M., Stutts, M. J., and Milgram, S. L. (2005). Phosphodiesterase 4D forms a cAMP diffusion barrier at the apical membrane of the airway epithelium. J. Biol. Chem. *280*, 7997–8003.

Barnette, M. S. (1999). Phosphodiesterase 4 (PDE4) inhibitors in asthma and chronic obstructive pulmonary disease (COPD). Prog. Drug. Res. *53*, 193–229.

Bates, I. R., Hebert, B., Luo, Y., Liao, J., Bachir, A. I., Kolin, D. L., Wiseman, P. W., and Hanrahan, J. W. (2006). Membrane lateral diffusion and capture of CFTR within transient confinement zones. Biophys. J. *91*, 1046–1058.

Bear, C. E., Li, C., Kartner, N., Bridges, R. J., Jensen, T. J., Ramjeesingh, M., and Riordan, J. R. (1992). Purification and functional reconstitution of the cystic fibrosis transmembrane conductance regulator (CFTR). Cell *68*, 809–818.

Beavo, J. A. (1995). Cyclic nucleotide phosphodiesterases: functional implications of multiple isoforms. Physiol. Rev. *75*, 725–748.

Buxton, I. L., and Brunton, L. L. (1983). Compartments of cAMP and protein kinase in mammalian cardiomyocytes. J. Biol. Chem. *258*, 10233–10239.

Cantiello, H. F. (1996). Role of the actin cytoskeleton in the regulation of the cystic fibrosis transmembrane conductance regulator. Exp. Physiol. *81*, 505–514.

Chasan, B., Geisse, N. A., Pedatella, K., Wooster, D. G., Teintze, M., Carattino, M. D., Goldmann, W. H., and Cantiello, H. F. (2002). Evidence for direct interaction between actin and the cystic fibrosis transmembrane conductance regulator. Eur. Biophys. J. *30*, 617–624.

Chen, Y., Lagerholm, B. C., Yang, B., and Jacobson, K. (2006). Methods to measure the lateral diffusion of membrane lipids and proteins. Methods *39*, 147–153.

Choi, J. Y., Joo, N. S., Krouse, M. E., Wu, J. V., Robbins, R. C., Ianowski, J. P., Hanrahan, J. W., and Wine, J. J. (2007). Synergistic airway gland mucus secretion in response to vasoactive intestinal peptide and carbachol is lost in cystic fibrosis. J. Clin. Invest. *117*, 3118–3127.

Chung, K. F. (2006). Phosphodiesterase inhibitors in airway disease. Eur. J. Pharmacol. *533*, 110–117.

Cobb, B. R., Fan, L., Kovacs, T. E., Sorscher, E. J., and Clancy, J. P. (2003). Adenosine receptors and phosphodiesterase inhibitors stimulate Cl− secretion in Calu-3 cells. Am. J. Respir. Cell. Mol. Biol. *29*, 410–418.

Compton, C. H., Gubb, J., Nieman, R., Edelson, J., Amit, O., Bakst, A., Ayres, J. G., Creemers, J. P., Schultze-Werninghaus, G., Brambilla, C., and Barnes, N. C. (2001). Cilomilast, a selective phosphodiesterase-4 inhibitor for treatment of patients with chronic obstructive pulmonary disease: a randomised, dose-ranging study. Lancet *358*, 265–270.

Conti, M., and Beavo, J. (2007). Biochemistry and physiology of cyclic nucleotide phosphodiesterases: essential components in cyclic nucleotide signaling. Annu. Rev. Biochem. *76*, 481–511.

Cooper, D. M. (2005). Compartmentalization of adenylate cyclase and cAMP signalling. Biochem. Soc. Trans. *33*, 1319–1322.

Dahan, M., Lévi, S., Luccardini, C., Rostaing, P., Riveau, B., and Triller, A. (2003). Diffusion dynamics of glycine receptors revealed by single-quantum dot tracking. Science *302*, 442–445.

Degerman, E., Belfrage, P., and Manganiello, V. C. (1997). Structure, localization, and regulation of cGMP-inhibited phosphodiesterase (PDE3). J. Biol. Chem. *272*, 6823–6826.

Galperin, E., and Sorkin, A. (2003). Visualization of Rab5 activity in living cells by FRET microscopy and influence of plasma-membrane-targeted Rab5 on clathrin-dependent endocytosis. J. Cell Sci. *116*, 4799–4810.

Ganeshan, R., Nowotarski, K., Di, A., Nelson, D. J., and Kirk, K. L. (2007). CFTR surface expression and chloride currents are decreased by inhibitors of N-WASP and actin polymerization. Biochim. Biophys. Acta *1773*, 192–200.

Giembycz, M. A., Corrigan, C. J., Seybold, J., Newton, R., and Barnes, P. J. (1996). Identification of cyclic AMP phosphodiesterases 3, 4 and 7 in human CD4+ and CD8+ T-lymphocytes: role in regulating proliferation and the biosynthesis of interleukin-2. Br. J. Pharmacol. *118*, 1945–1958.

Giembycz, M. A. (2005). Phosphodiesterase-4, selective and dual-specificity inhibitors for the therapy of chronic obstructive pulmonary disease. Proc. Am. Thorac. Soc. *2*, 326–333.

Halpin, D. M. (2008). ABCD of the phosphodiesterase family: interaction and differential activity in COPD. Int. J. Chron. Obstruct. Pulmon. Dis. *3*, 543–561.

Huang, P., Lazarowski, E. R., Tarran, R., Milgram, S. L., Boucher, R. C., and Stutts, M. J. (2001). Compartmentalized autocrine signaling to cystic fibrosis transmembrane conductance regulator at the apical membrane of airway epithelial cells. Proc. Natl. Acad. Sci. USA *98*, 14120–14125.

Ianowski, J. P., Choi, J. Y., Wine, J. J., and Hanrahan, J. W. (2008). Substance P stimulates CFTR-dependent fluid secretion by mouse tracheal submucosal glands. Pfluegers Arch. *457*, 529–537.

Jin, S., Haggie, P. M., and Verkman, A. S. (2007). Single-particle tracking of membrane protein diffusion in a potential: simulation, detection, and application to confined diffusion of CFTR Cl− channels. Biophys. J. *93*, 1079–1088.

Joo, N. S., Wu, J. V., Krouse, M. E., Saenz, Y., and Wine, J. J. (2001). Optical method for quantifying rates of mucus secretion from single submucosal glands. Am. J. Physiol. Lung Cell Mol. Physiol. *281*, L458–L468.

Kelley, T. J., Al-Nakkash, L., and Drumm, M. L. (1995). CFTR-mediated chloride permeability is regulated by type III phosphodiesterases in airway epithelial cells. Am. J. Respir. Cell. Mol. Biol. *13*, 657–664.

Kelley, T. J., Thomas, K., Milgram, L. J., and Drumm, M. L. (1997). In vivo activation of the cystic fibrosis transmembrane conductance regulator mutant deltaF508 in murine nasal epithelium. Proc. Natl. Acad. Sci. USA *94*, 2604–2608.

Langeberg, L. K., and Scott, J. D. (2005). A-kinase-anchoring proteins. J. Cell Sci. *118*, 3217–3220.

Lee, J. H., Richter, W., Namkung, W., Kim, K. H., Kim, E., Conti, M., and Lee, M. G. (2007). Dynamic regulation of cystic fibrosis transmembrane conductance regulator by competitive interactions of molecular adaptors. J. Biol. Chem. *282*, 10414–10422.

Li, C., *et al.* (2005). Lysophosphatidic acid inhibits cholera toxin-induced secretory diarrhea through CFTR-dependent protein interactions. J. Exp. Med. *202*, 975–986.

Li, C., Krishnamurthy, P. C., Penmatsa, H., Marrs, K. L., Wang, X. Q., Zaccolo, M., Jalink, K., Li, M., Nelson, D. J., Schuetz, J. D., and Naren, A. P. (2007). Spatiotemporal coupling of cAMP transporter to CFTR chloride channel function in the gut epithelia. Cell *131*, 940–951.

Li, C., and Naren, A. P. (2005). Macromolecular complexes of cystic fibrosis transmembrane conductance regulator and its interacting partners. Pharmacol. Ther. *108*, 208–223.

Li, C., Roy, K., Dandridge, K., and Naren, A. P. (2004). Molecular assembly of cystic fibrosis transmembrane conductance regulator in plasma membrane. J. Biol. Chem. *279*, 24673–24684.

Liu, S., *et al.* (2005). Dynamic activation of cystic fibrosis transmembrane conductance regulator by type 3 and type 4D phosphodiesterase inhibitors. J. Pharmacol. Exp. Ther. *314*, 846–854.

Liu, Y., Shakur, Y., Yoshitake, M., and Kambayashi Ji, J. (2001). Cilostazol (pletal): a dual inhibitor of cyclic nucleotide phosphodiesterase type 3 and adenosine uptake. Cardiovasc. Drug Rev. *19*, 369–386.

McConnachie, G., Langeberg, L. K., and Scott, J. D. (2006). AKAP signaling complexes: getting to the heart of the matter. Trends Mol. Med. *12*, 317–323.

Meacci, E., Taira, M., Moos, M., Jr., Smith, C. J., Movsesian, M. A., Degerman, E., Belfrage, P., and Manganiello, V. (1992). Molecular cloning and expression of human myocardial cGMP-inhibited cAMP phosphodiesterase. Proc. Natl. Acad. Sci. USA *89*, 3721–3725.

Naren, A. P., *et al.* (2003). A macromolecular complex of beta 2 adrenergic receptor, CFTR, and ezrin/radixin/moesin-binding phosphoprotein 50 is regulated by PKA. Proc. Natl. Acad. Sci. USA *100*, 342–346.

O'Grady, S. M., Jiang, X., Maniak, P. J., Birmachu, W., Scribner, L. R., Bulbulian, B., and Gullikson, G. W. (2002). Cyclic AMP-dependent Cl secretion is regulated by multiple phosphodiesterase subtypes in human colonic epithelial cells. J. Membr. Biol. *185*, 137–144.

Perry, S. J., *et al.* (2002). Targeting of cyclic AMP degradation to β_2-adrenergic receptors by β-arrestins. Science *298*, 834–836.

Pilewski, J. M., and Frizzell, R. A. (1999). Role of CFTR in airway disease. Physiol. Rev. *79*, S215–S255.

Ponsioen, B., Zhao, J., Riedl, J., Zwartkruis, F., Van der Krogt, G., Zaccolo, M., Moolenaar, W. H., Bos, J. L., and Jalink, K. (2004). Detecting cAMP-induced Epac activation by fluorescence resonance energy transfer: Epac as a novel cAMP indicator. EMBO Rep. *5*, 1176–1180.

Pozuelo Rubio, M., Campbell, D. G., Morrice, N. A., and Mackintosh, C. (2005). Phosphodiesterase 3A binds to 14-3-3 proteins in response to PMA-induced phosphorylation of Ser428. Biochem. J. *392*, 163–172.

Puxeddu, E., Uhart, M., Li, C. C., Ahmad, F., Pacheco-Rodriguez, G., Manganiello, V. C., Moss, J., and Vaughan, M. (2009). Interaction of phosphodiesterase 3A with brefeldin A-inhibited guanine nucleotide-exchange proteins BIG1 and BIG2 and effect on ARF1 activity. Proc. Natl. Acad. Sci. USA *106*, 6158–6163.

Riordan, J. R. (2008). CFTR function and prospects for therapy. Annu. Rev. Biochem. *77*, 701–726.

Riordan, J. R., *et al*. (1989). Identification of the cystic fibrosis gene: cloning and characterization of complementary DNA. Science *245*, 1066–1073.

Rogers, C. S., *et al.* (2008). Disruption of the CFTR gene produces a model of cystic fibrosis in newborn pigs. Science *321*, 1837–1841.

Schudt, C., Tenor, H., and Hatzelmann, A. (1995). PDE isoenzymes as targets for anti-asthma drugs. Eur. Respir. J. *8*, 1179–1183.

Shakur, Y., Holst, L. S., Landstrom, T. R., Movsesian, M., Degerman, E., and Manganiello, V. (2001). Regulation and function of the cyclic nucleotide phosphodiesterase (PDE3) gene family. Prog. Nucleic Acid Res. Mol. Biol. *66*, 241–277.

Sheppard, D. N., and Welsh, M. J. (1999). Structure and function of the CFTR chloride channel. Physiol. Rev. *79*, S23–S45.

Shin, D. D., Brandimarte, F., De Luca, L., Sabbah, H. N., Fonarow, G. C., Filippatos, G., Komajda, M., and Gheorghiade, M. (2007). Review of current and investigational pharmacologic agents for acute heart failure syndromes. Am. J. Cardiol. *99*, 4A–23A.

Smith, F. D., Langeberg, L. K., and Scott, J. D. (2006). The where's and when's of kinase anchoring. Trends. Biochem. Sci. *31*, 316–323.

Taskén, K. A., Collas, P., Kemmner, W. A., Witczak, O., Conti, M., and Taskén, K. (2001). Phosphodiesterase 4D and protein kinase a type II constitute a signaling unit in the centrosomal area. J. Biol. Chem. *276*, 21999–22002.

Thompson, P. E., Manganiello, V., and Degerman, E. (2007). Re-discovering PDE3 inhibitors—new opportunities for a long neglected target. Curr. Top. Med. Chem. *7*, 421–436.

Torphy, T. J. (1998). Phosphodiesterase isozymes: molecular targets for novel antiasthma agents. Am. J. Respir. Crit. Care Med. *157*, 351–370.

Ullman, E. F., *et al.* (1996). Luminescent oxygen channeling assay (LOCI): sensitive, broadly applicable homogeneous immunoassay method. Clin. Chem. *42*, 1518–1526.

Wine, J. J., and Joo, N. S. (2004). Submucosal glands and airway defense. Proc. Am. Thorac. Soc. *1*, 47–53.

Wright, L. C., Seybold, J., Robichaud, A., Adcock, I. M., and Barnes, P. J. (1998). Phosphodiesterase expression in human epithelial cells. Am. J. Physiol. *275*, L694–L700.

Yoo, D., Flagg, T. P., Olsen, O., Raghuram, V., Foskett, J. K., and Welling, P. A. (2004). Assembly and trafficking of a multiprotein ROMK (Kir 1.1) channel complex by PDZ interactions. J. Biol. Chem. *279*, 6863–6873.

Zaccolo, M., and Pozzan, T. (2002). Discrete microdomains with high concentration of cAMP in stimulated rat neonatal cardiac myocytes. Science *295*, 1711–1715.

Zaccolo, M. (2006). Phosphodiesterases and compartmentalized cAMP signalling in the heart. Eur. J. Cell Biol. *85*, 693–697.